Proceedings World Geothermal Congress 2020+1
Reykjavik, Iceland, April - October 2021

Development of a Transient, Multi-Feed Geothermal Wellbore Simulator

Ryan Tonkin, John O'Sullivan and Michael O'Sullivan

Department of Engineering Science, University of Auckland, Auckland, New Zealand

rton671@aucklanduni.ac.nz

Keywords: well, multi-feed, transient, two-phase, simulation, validation

ABSTRACT

Simulation of the flow in a geothermal wellbore is an important reservoir engineering task, however, most existing geothermal wellbore simulators can only deal with steady-state conditions. This paper discusses the theoretical background and numerical implementation of a transient geothermal wellbore model that is currently under development. The simulator is capable of modelling transient single and two-phase flow in wells with multiple feed-zones. A geothermal wellbore simulator solves the conservation of mass, momentum, and energy equations that govern flow in a geothermal wellbore. These, along with the additional equations required for model closure, are presented. The governing equations are discretized and solved numerically using a fully implicit Newton-Raphson procedure for pressure, temperature (swapped with saturation for two-phase conditions), vapour velocity, and liquid volume flux as primary variables. The implementation of the simulator is tested using analytical solutions for simplified single-phase flow situations. Steady-state validation cases are presented for both single-feed and multi-feed wellbores. Finally, a simulation of the transient behavior of geothermal production well is presented as a test case, and further applications of the simulator are discussed.

1. INTRODUCTION

Wellbores play a critical role in the exploitation and management of geothermal systems. They form the link between the subsurface geothermal system and the energy production facilities on the surface. The direct monitoring and analysis of geothermal wellbores provides vital information about their behavior (Axelsson, 2013). However, the harsh operating conditions, as well as the expense and complexity of running flowing surveys in geothermal wells, often prevent the installation of measuring equipment (Upadhyay et al., 1977). Therefore, geothermal wellbore models provide an invaluable tool for inferring the characteristics of geothermal wellbores and predicting their future behavior.

Many steady-state wellbore models exist, e.g., HOLA (Bjornsson, 1987; Aunzo et al., 1991), WELLSIM (Gunn and Freeston, 1992), SWELFLOW/SIMGWELL, (McGuiness, 2015; Marquez et al., 2015), FLOWELL (Gudmundsdottir and Jonsson, 2015). However, there are comparatively few past applications of transient geothermal wellbore simulation. Some of the transient processes associated with output tests have been studied by simulation (Miller, 1980a; Miller et al. 1982; Khasani et al., 2017). Recently, transient simulations of geothermal wells have investigated the impact of multiple feeds on production testing (Vasini et al., 2018), well cycling (Yamamura et al. 2016; Yamamura et al., 2017, Itoi et al. 2013), and airlifting during wellbore startup (Akbar et al., 2016).

This study describes the theoretical background and implementation of a new transient wellbore simulator. Multi-phase fluid flow in a geothermal wellbore is governed by three fundamental laws: the conservation of mass, conservation of momentum, and the conservation of energy. These are presented in Section 2, along with the additional constitutive equations required for model closure. These conservation equations are non-linear and must be solved numerically. The discrete conservation equations and the numerical solution procedure used to solve them are discussed in Sections 3 and 4, respectively. The verification and validation of the simulator against simple analytical solutions and flowing pressure-temperature logs are presented in Sections 5 and 6. Finally, an example of a transient, multi-feed simulation is given in Section 7 and future modelling challenges are discussed in Section 8.

2. MATHEMATICAL MODEL FORMULATION

2.1 Two-Phase Conservation Equations

The governing equations for the three-equation model for fluid flow in a deviated geothermal wellbore, with a variable cross-sectional area are given by Equations (1), (2) and (3) below. They describe the behavior of the fluid as a mixture rather than dealing with each phase individually, however, the equations are written in terms of separate quantities for each phase. This formulation ensures that effects of phase slip on momentum and energy transport are accounted for. The assumptions made in the derivation of this model are:

- 1-D flow – flow variables are averaged across the well cross-section
- equal pressure in each phase
- negligible axial heat conduction
- the two phases are in local thermodynamic equilibrium
- the existence of a relationship between the velocities of liquid and gas (slip relationship)
- the effects of non-condensable gases and dissolved salts are not considered

The conservation of mass for a two-phase mixture is:

$$\frac{\partial}{\partial t}[\rho_v S_v + \rho_l S_l] + \frac{1}{A}\frac{\partial}{\partial s}[A\rho_v S_v u_v + A\rho_l S_l u_l] - q_{mass} = 0. \quad (1)$$

Here, the subscripts *l* and *v* are used for the liquid and vapour phases, respectively, and then S_l and S_v are the saturations, u_l and u_v are the velocities, and ρ_l and ρ_v are the densities. The independent variable, *s*, is the distance up the wellbore, *A* is the cross-sectional area of the well, and q_{mass} represents external sources of mass from feed-zones.

The equation governing conservation of momentum is:

$$\frac{\partial}{\partial t}[\rho_v S_v u_v + \rho_l S_l u_l] + \frac{1}{A}\frac{\partial}{\partial s}[A\rho_v S_v {u_v}^2 + A\rho_l S_l {u_l}^2] + \frac{\partial P}{\partial s} + \frac{2}{r}\tau + (\rho_v S_v + \rho_l S_l) g \frac{\partial z}{\partial s} - q_{mom} = 0. \quad (2)$$

Here, *P* is the wellbore pressure, *g* is the gravitational acceleration, and τ is the wellbore friction term. The variable *r* is wellbore radius, and *z* is the vertical elevation of the well segment. The external source or sink of momentum is given by q_{mom}.

The conservation of energy equation is:

$$\frac{\partial}{\partial t}\left[\rho_v S_v \left(h_v + \frac{1}{2}{u_v}^2\right) + \rho_l S_l \left(h_l + \frac{1}{2}{u_l}^2\right) - P\right] + \frac{1}{A}\frac{\partial}{\partial s}\left[A\rho_v S_v u_v \left(h_v + \frac{1}{2}{u_v}^2\right) + A\rho_l S_l u_l \left(h_l + \frac{1}{2}{u_l}^2\right)\right] + (\rho_v S_v u_v + \rho_l S_l u_l) g \frac{\partial z}{\partial s} + q_{heat} - q_{ener} = 0. \quad (3)$$

Here, it is given in terms of the enthalpy and kinetic energy of each phase. The term q_{heat} is the heat flux away from the wellbore into the formation due to conduction, and q_{ener} represents the net energy transported into or out of the well by sources or sinks. The enthalpy of each phase is given by h_v and h_l.

2.2 Constitutive Equations

The conservation laws (1), (2) and (3) have more unknowns than the number of equations and supplementary constitutive equations are required to complete the set. There is a wide range of constitutive models to choose from and the selection made has a significant impact on simulation results (Akbar et al, 2016). The constitutive models for phase slip, heat flux, friction, and source terms are discussed below.

2.2.1 Phase Slip

Three-equation models for two-phase flow require an additional constitutive equation to model phase slip. This simulator uses the drift flux model originally presented by Zuber and Findlay (1965) and used in some past transient simulators. Pan et al. (2011) solved equations (4) and (5) below for the phase velocities while Garcia-Valladares et al. (2006) and Akbar et al. (2016) solved the drift flux model for vapour saturation.

The vapour and liquid velocities are calculated using the drift flux model by:

$$u_v = C_0 F_V + u_d, \quad (4)$$

and

$$u_l = \frac{1 - S_v C_0}{1 - S_v} F_V - \frac{S_v}{1 - S_v} u_d. \quad (5)$$

In (4) and (5), F_V is the total volume flux, also called the velocity of the center of volume and is defined as $F_V = S_v u_v + S_l u_l$.

The distribution coefficient, C_0, accounts for non-uniform saturation and volume flux profiles across the well, while the drift velocity, u_d, accounts for the relative velocity between phases caused by buoyancy forces (Yadigaroglu, 2018). Empirical equations are required for both C_0 and u_d. The simplest constitutive model for slip assumes that the phase velocities are equal and is called homogeneous flow. The drift-flux formulation for this model is $u_d = 0$ and $C_0 = 1$. However, homogeneous flow is not generally applicable across the range of conditions possible within a wellbore.

Instead, Pan et al.'s (2011) constitutive model for C_0 and u_d is used in this simulator. This was adapted from the model presented by Shi et al. (2005) and has been shown to produce good results in geothermal applications (Vasini et al. 2018; Pan et al., 2015). However, García-Valladares et al. (2006) and Akbar et al. (2016) both suggest that the choice of the slip relationship has a large effect on the results of wellbore simulation and further research is required to determine the best slip relations for transient geothermal well applications. Our simulator is written in a general form and can easily be modified to include other slip models.

2.2.2 Wellbore Friction

A constitutive equation is required for modelling the friction force between the geothermal fluid and wellbore wall. A two-phase form of the classical Darcy–Weisbach equation is used:

$$\frac{2}{r}\tau = \frac{1}{4r} f F_m \left|\frac{F_m}{S_v\rho_v + S_l\rho_l}\right|. \quad (6)$$

Here, the total mass flux F_m is the sum of the mass fluxes for each phase:

$$F_m = F_{mv} + F_{ml} = S_v\rho_v u_v + S_l\rho_l u_l. \quad (7)$$

The Darcy friction factor, f, is calculated using the Colebrook-White equation and is a function of pipe roughness and the two-phase Reynolds number (Re), which is calculated as:

$$Re = \frac{F_m d}{S_v \mu_v + S_l \mu_l}. \quad (8)$$

Here, d is the well diameter and μ_v and μ_l are the dynamic viscosities of the vapour and liquid phases.

This model for friction was chosen for both its simplicity and because it varies smoothly across all phase states. Additionally, it has been used in transient geothermal models by Pan et al. (2014) and Akbar et al. (2016). Older transient simulators (Miller 1980; Garcia-Valladares et al., 2006) have calculated friction losses using "two-phase multiplier" methods. This method multiplies the single-phase version of (6), calculated with the properties of the liquid phase, by an empirical term (Chisholm, 1973; Beattie, 1973).

2.2.3 Wellbore Heat Loss

The heat loss from the wellbore to the reservoir due to conduction, q_{heat}, is modelled using Ramey's equation for heat loss (Ramey, 1962, Horne and Shinohara, 1979):

$$q_{heat} = \frac{2}{r} \frac{k_{res} U (T_{wb} - T_{res})}{k_{res} + rUf(t_D)}. \quad (9)$$

Here, the dimensionless time is defined as $t_D = \alpha t / r_c^2$ where $\alpha = k_{res}/\rho_{res} c_{res}$ and r_c is the radius of the cement-reservoir interface, and k_{res}, ρ_{res} and c_{res} are the thermal conductivity, density, and specific heat capacity of the reservoir. T_{res} is the formation temperature, T_{wb} is the wellbore temperature, and U is the over-all heat transfer coefficient. The time function, $f(t_D)$, approximates the transient nature of wellbore-formation heat exchange. Chiu and Thakur's (1991) version of the time function is given by:

$$f(t_D) = 0.982 \ln(1 + 1.81 t_D). \quad (10)$$

This formula has been shown to provide a reasonable approximation of transient wellbore-reservoir heat exchange (Vasini et al., 2018) while avoiding the early time discontinuity that results from using Ramey's (1962) original time function.

Willhite (1967) provided a general expression for the term U in (9), that describes the thermal resistance of any wellbore completion. For the present study, Willhite's (1967) equation was simplified to only include the effects of a single cemented annulus, and thus:

$$U = \frac{k_c}{r \ln(r_c/r)}. \quad (11)$$

Here, k_c is the thermal conductivity of the cement, r is the wellbore radius, and r_c is the radius of the cement-reservoir interface.

2.2.4 Source Terms

The source terms q_{mass}, q_{mom} and q_{ener} in (1), (2) and (3) describe the mass, momentum, and energy transfer between feed-zones and the wellbore. The total source of mass is the sum of the liquid and vapour components:

$$q_{mass} = q_{mv} + q_{ml}. \quad (12)$$

The reservoir mass flux for each fluid phase, $q_{m\beta}$, is calculated using a deliverability equation based on two-phase Darcy flow:

$$q_{m\beta} = \frac{k_{r\beta}}{\nu_\beta} \mathrm{PI}(P_{res} - P_{wb})/V. \quad (13)$$

Here, $k_{r\beta}$ and υ_β are the relative permeability and kinematic viscosity of each phase, PI is the productivity index of the feed, P_{res} is a prescribed reservoir pressure, P_{wb} is the pressure in the well at the depth of the feedzone, and $V = \pi r^2 \Delta s$ is the volume of the wellbore element. Combining (12) and (13), the total mass input can be written in terms of a lumped parameter, α:

$$q_{mass} = \alpha(P_{res} - P_{wb})/V. \quad (14)$$

The source of energy in Equation (3) is modelled as:

$$q_{ener} = q_{mass} h_{fres}, \quad (15)$$

in which h_{fres} is the flowing enthalpy of the feed:

$$h_{fres} = \frac{\frac{h_l k_{rl}}{\nu_l} + \frac{h_v k_{rv}}{\nu_v}}{\frac{k_{rl}}{\nu_l} + \frac{k_{rv}}{\nu_v}}. \quad (16)$$

Here, h_l and h_v are the enthalpies of the feedzone fluid.

Finally, the fluid from the feed is assumed to enter the well perpendicular to the direction of flow (Bendikson et al., 1991). Therefore, there is no net transfer of momentum, meaning $q_{mom} = 0$ in (2).

2.2.5 Thermodynamic Properties

The properties of pure water are calculated using the revised IAPWS industrial formulation 1997 (Wagner et al., 2000). The surface tension is calculated using the IAPWS revised correlation (2014).

3. NUMERICAL IMPLEMENTATION

Analytical solution of the non-linear mass, momentum, and energy conservation equations is not possible and they must be solved numerically. To do this, the governing equations presented in Section 2 are discretized and solved for the primary thermodynamic variables using the Newton-Raphson method. An outline of this numerical method is given in Section 4. The primary variables for this simulator were chosen as pressure, temperature (swapped with vapour saturation for two-phase conditions), vapour velocity, and liquid volume flux. These were found to provide the best numerical performance over a range of test problems for the model described in this work (Tonkin et al., 2020).

A fully implicit, one-dimensional finite volume discretization is used in this simulator. Here, static wellbore properties, e.g., pressure, temperature, and saturation, are defined at the center of a wellbore element, as shown in Figure 1 a), whereas flowing variables, e.g., fluid velocity and fluxes are defined on the element boundaries, as shown in Figure 1 b).

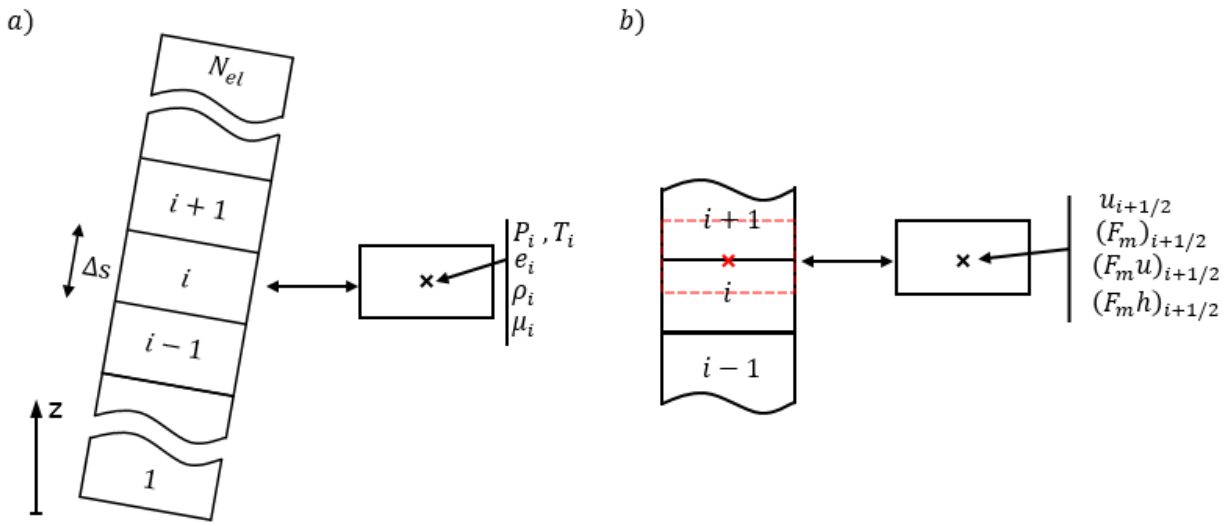

Figure 1: Wellbore discretization scheme and variable definitions for a) the mass and energy equations centered on element i and b) the momentum equation centered on the interface between elements at $i + 1/2$

The discretized mass equation is presented in residual form below:

$$\frac{1}{\Delta t}\left([S_v\rho_v + S_l\rho_l]_i^{n+1} - [S_v\rho_v + S_l\rho_l]_i^{n}\right) + \frac{1}{[V]_i}\left([AF_{mv} + AF_{ml}]_{i+1/2}^{n+1} - [AF_{mv} + AF_{ml}]_{i-1/2}^{n+1}\right) - [q_{mass}]_i^{n+1} = 0 \tag{17}$$

Here, the superscripts $n+1$ and n indicate the current and previous time steps, respectively. The subscript i is the spatial index of an element center. The subscript $i+1/2$ is the index of the interface between elements i and $i+1$. The time step is Δt, and the volume of a wellbore block is $[V]_i$, defined as:

$$[V]_i = [A]_i \Delta s_i \tag{18}$$

where $[A]_i$ is the average cross-sectional area and Δs_i is the axial length of a wellbore element.

The mass flux of a phase on an interface is defined as:

$$[F_{m\beta}]_{i+1/2}^{n+1} = [\rho_\beta S_\beta]_{i+1/2}^{n+1} [u_\beta]_{i+1/2}^{n+1} \tag{19}$$

Equation (19) requires values of saturation and density on the interface, however, they are defined at the center of a cell. The interface saturation and density are weighted according to the direction of the flow, a method called upstream weighting or upwinding. The interface saturation is calculated using:

$$[S_\beta]_{i+1/2}^{n+1} \begin{cases} [S_\beta]_i^{n+1}, & [X_\beta]_{i+1/2}^{n+1} \geq 0 \\ [S_\beta]_{i+1}^{n+1}, & [X_\beta]_{i+1/2}^{n+1} < 0 \end{cases}, \tag{20}$$

and the interface density is calculated using:

$$[\rho_\beta]_{i+1/2}^{n+1} \begin{cases} [\rho_\beta]_i^{n+1}, & [X_\beta]_{i+1/2}^{n+1} \geq 0 \\ [\rho_\beta]_{i+1}^{n+1}, & [X_\beta]_{i+1/2}^{n+1} < 0 \end{cases}. \tag{21}$$

Here, $[X_\beta]_{i+1/2}^{n+1}$ refers to the flowing primary variable of a phase. These are either the vapour velocity or liquid volume flux.

In (19), the velocity of the vapour phase is calculated as a primary variable. However, the liquid velocity is calculated as a secondary variable from the liquid volume flux:

$$[u_l]_{i+1/2}^{n+1} = \begin{cases} [F_{Vl}]_{i+1/2}^{n+1} / [S_l]_{i+1/2}^{n+1} & , [S_l]_{i+1/2}^{n+1} \neq 0 \\ 0 & , [S_l]_{i+1/2}^{n+1} = 0 \end{cases}. \tag{22}$$

Here, $[S_l]_{i+1/2}^{n+1}$ is the upwinded interface saturation defined in (20).

The momentum control element, shown in red in Figure 2 b), is centered on the interface between two elements. This discrete conservation of momentum is:

$$\frac{1}{\Delta t}\left([F_{mv} + F_{ml}]_{i+1/2}^{n+1} - [F_{mv} + F_{ml}]_{i+1/2}^{n}\right) +$$

$$\frac{1}{[V]_{i+\frac{1}{2}}} \begin{cases} [AF_{mv}u_v]_{i+1/2}^{n+1} - [AF_{mv}u_v]_{i-1/2}^{n+1}, & [u_v]_{i+1/2}^{n+1} \geq 0 \\ [AF_{mv}u_v]_{i+3/2}^{n+1} - [AF_{mv}u_v]_{i+1/2}^{n+1}, & [u_v]_{i+1/2}^{n+1} < 0 \end{cases} + \frac{1}{[V]_{i+\frac{1}{2}}} \begin{cases} [AF_{ml}u_l]_{i+1/2}^{n+1} - [AF_{ml}u_l]_{i-1/2}^{n+1}, & [F_{Vl}]_{i+1/2}^{n+1} \geq 0 \\ [AF_{ml}u_l]_{i+3/2}^{n+1} - [AF_{ml}u_l]_{i+1/2}^{n+1}, & [F_{Vl}]_{i+1/2}^{n+1} < 0 \end{cases}$$

$$+ \frac{P_{i+1}^{n+1} - P_i^{n+1}}{s_{i+1} - s_i} + \frac{2}{R}\tau_{i+1/2}^{n+1} + [\rho_v S_v + \rho_l S_l]_{i+1/2}^{n+1} g \frac{z_{i+1} - z_i}{s_{i+1} - s_i} - [q_{mom}]_{i+1/2}^{n+1} = 0 \tag{23}$$

In (23), the momentum flux difference, given in terms 2 and 3, are upwinded based on the phase velocities at $1 + 1/2$.

The gravity term in (23) uses the average density on the interface,

$$[\rho_v S_v + \rho_l S_l]_{i+1/2}^{n+1} = \frac{1}{2}\left([\rho_v S_v + \rho_l S_l]_i^{n+1} + [\rho_v S_v + \rho_l S_l]_{i+1}^{n+1}\right) \tag{24}$$

Equation (24) must be used instead of the upwinded saturations and densities. This is because in simulations with low mass flow the liquid velocity can flip between positive and negative values after each Newton iteration. This causes the value of the gravity term to change and can result in slow, and sometimes failed, convergence.

The effective interface volume, $[V]_{i+1/2}$, is the average volume of the surrounding elements:

$$[V]_{i+1/2} = \frac{1}{2}([V]_{i+1} + [V]_i). \tag{25}$$

The discretized energy conservation equation is:

$$\frac{1}{\Delta t}\left([S_v\rho_v H_v + S_l\rho_l H_l - P]_i^{n+1} - [S_v\rho_v H_v + S_l\rho_l H_l - P]_i^{n}\right)$$

$$+ \frac{1}{[V]_i}\left([AF_{mv}H_v + AF_{ml}H_l]_{i+1/2}^{n+1} - [AF_{mv}H_v + AF_{ml}H_l]_{i-1/2}^{n+1}\right)$$

$$+ [F_{mv} + F_{ml}]_i^{n+1} g \frac{z_{i+1} - z_{i-1}}{s_{i+1} - s_{i-1}} + [q_{heat}]_i^{n+1} - [q_{ener}]_i^{n+1} = 0 \tag{26}$$

Here H_β is the sum of the enthalpy and kinetic energy of each phase:

$$\left[H_\beta\right]_i^{n+1} = \left[h_\beta\right]_i^{n+1} + \left[E_{K\beta}\right]_i^{n+1} \tag{27}$$

where $\left[E_{K\beta}\right]_i^{n+1}$ is the average kinetic energy of a phase. It is defined as the average of the kinetic energy at the interfaces,

$$\left[E_{K\beta}\right]_i^{n+1} = \frac{1}{2}\left(\frac{1}{2}\left[u_\beta^2\right]_{i+1/2}^{n+1} + \frac{1}{2}\left[u_\beta^2\right]_{i-1/2}^{n+1}\right). \tag{28}$$

The interface enthalpies are upstream weighted, such that:

$$\left[H_\beta\right]_{i+1/2}^{n+1} \begin{cases} \left[H_\beta\right]_i^{n+1}, & \left[X_\beta\right]_{i+1/2}^{n+1} \geq 0 \\ \left[H_\beta\right]_{i+1}^{n+1}, & \left[X_\beta\right]_{i+1/2}^{n+1} < 0 \end{cases}. \tag{29}$$

The mass flux at *i* is:

$$\left[F_{m\beta}\right]_i^{n+1} = \left[\rho_\beta S_\beta\right]_i^{n+1}\left[u_\beta\right]_i^{n+1}. \tag{30}$$

Here, the average velocity at *i* is calculated differently depending on the phase. The vapour velocity is calculated as:

$$[u_v]_i^{n+1} = \frac{1}{2}\left([u_v]_{i+1/2}^{n+1} + [u_v]_{i-1/2}^{n+1}\right), \tag{31}$$

and the liquid velocity is calculated as:

$$[u_l]_i^{n+1} = \frac{1}{2}\left([F_{Vl}]_{i+1/2}^{n+1} + [F_{Vl}]_{i-1/2}^{n+1}\right) / [S_l]_i^{n+1}. \tag{32}$$

Finally, the constitutive equation for slip is solved implicitly. For a two-phase interface, the discrete form of (4) is solved:

$$[u_v]_{i+\frac{1}{2}}^{n+1} - [C_0]_{i+\frac{1}{2}}^{n+1}[F_V]_{i+\frac{1}{2}}^{n+1} - [u_d]_{i+\frac{1}{2}}^{n+1} = 0. \tag{33}$$

When an interface is single-phase, the velocity or volume flux of the non-present phase set to zero.

4. SOLUTION PROCEEDURE

The discrete conservation equations discussed above are non-linear and strongly coupled. They are solved simultaneously using Newton-Raphson iterations. This method iteratively updates the primary variable vector, x, to drive the imbalance in the residual equations (e.g. (17), (23), (26) and (33)) to zero using the following linear system:

$$\mathbf{J}\Delta x = -R. \tag{34}$$

Here **J** is the Jacobian matrix, and R is the residual vector calculated using the discretised conservation equations. This linear system is solved for the update vector, Δx, representing the change in primary variables.

The Jacobian matrix is defined as:

$$J_{ij} = \frac{\partial R_i}{\partial x_j} = \frac{R_i(x_j + dx_j) - R_i(x_j)}{dx_j}. \tag{35}$$

It describes how the discrete residual equations given in Section 3 change with respect to the primary variables. It is used to drive the convergence of the residual equations to zero for each time step and, if not calculated accurately, can result in slow or failed convergence and erroneous solutions. Our simulator calculates the Jacobian using finite differencing. This involves perturbing the primary variable x_j by a small amount dx_j (scaled to the size of the primary variable) and taking the forward difference, as shown in (35). This method can be prone to truncation and round-off errors. Decreasing the step size, dx_j, will reduce the truncation error, however, it will also increase the round-off error. The optimal size of dx_j is unknown and differs for each residual equation. For this reason, dx_j is estimated as $dx_j = 1\text{E}-6 \times (x_j + 1)$.

5. MODEL VERIFICATION

Analytical solution can be derived for simplified forms of the single-phase conservation equations. These are used to check the numerical implementation of the simulator.

5.1 Test 1 - Constant Density Model

A simple linear model is derived by assuming steady-state flow of a single-phase isothermal fluid. The fluid density and frictional effects are assumed to be constant. Applying these assumptions to Equations (1) and (2) and integrating with respect to pressure gives:

$$P(z) = P_0 - z\left(\frac{f}{4r}\frac{F_m|F_m|}{\rho} + \rho g\right). \tag{36}$$

Here, P_0 is the wellhead pressure. The coefficient of friction, f, was fixed at 2.5e-2. Simulations were run for both liquid and vapour conditions in a 1500 m vertical wellbore with a diameter of 0.216 m, discretized into 10 elements. The fluid density was 988 kg/m^3 and 10 kg/m^3 for the liquid and vapour simulations, respectively. A constant pressure of 8 bar was set at the wellhead while the rate of mass flowing into the well through the bottom boundary was varied.

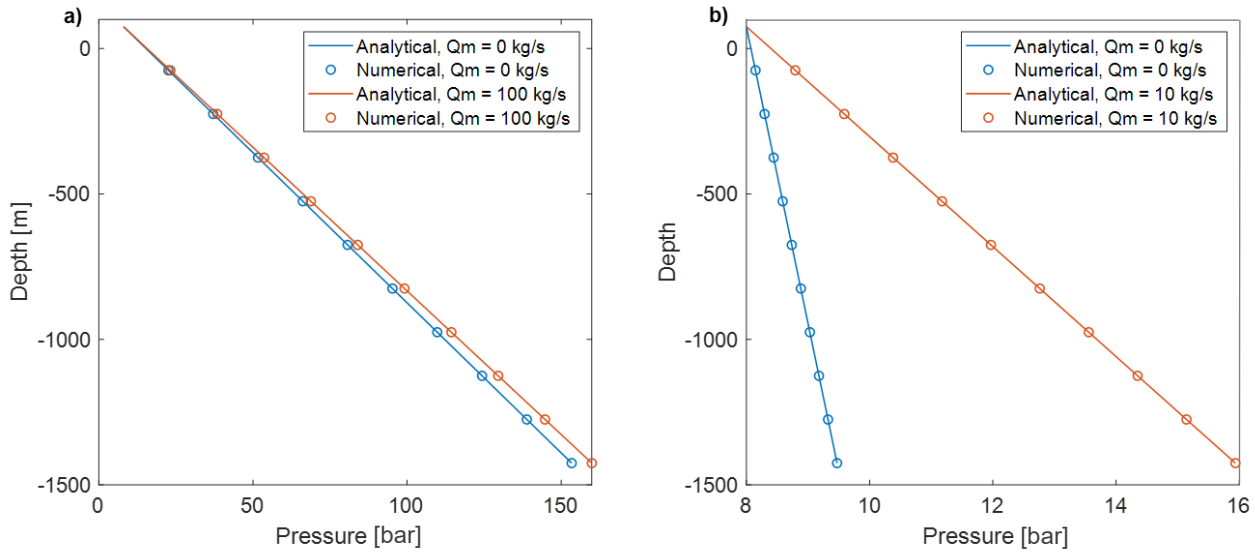

Figure 2: Numerical and analytical comparison for test case 1 for a) single-phase liquid and b) single-phase vapour

Figure 2 shows a good match between analytical model and numerical results for a variety of mass flow rates for both the liquid and vapour phases. Although simple, this problem helps to verify that the implementations of the gravitational and friction terms in the momentum equation are correct.

5.2 Test 2 - Linear Density Model

A second simple analytical solution was derived for a steady-state, single-phase isothermal fluid. The fluid density is assumed to be a linear function of pressure, such that $\rho = mP + c$, derived from the IAPWS-IF97 correlations, and friction effects are ignored. This is a simplified case of a semi-analytical solution presented by Pan et al. (2011). The following equation for the wellbore pressure gradient results from simplifying (1) and (2) using these assumptions.

$$\frac{dP}{dz} = -\frac{\rho g}{{F_m}^2 \frac{d}{dP}(1/\rho)+1}, \tag{37}$$

Inverting (36) and integrating with respect to pressure gives the following analytical expression for depth in terms of wellbore pressure:

$$z(P) = C - \frac{1}{mg} ln\,|\,\rho| - \frac{{F_m}^2}{2g}\frac{1}{\rho^2}, \tag{38}$$

where

$$C = \frac{1}{mg} ln\,|\,\rho_0| + \frac{{F_m}^2}{2g}\frac{1}{\rho(P_0)^2}. \tag{39}$$

Here, ρ_0 is the density calculated from the wellhead pressure, and m is the gradient of density with respect to pressure. The lengths of the wellbores were 4000m and 1500m for the liquid and vapour simulations, respectively. Both were discretized into 50 elements. Figure 3 a) presents the comparison between the analytical and numerical solutions for liquid water flowing at 20 kg.m^{-2}.s^{-1}.

A good match is achieved with a maximum relative error of 0.03% between the analytical and numerical calculations of depth. Changes in mass flux have little influence on the pressure profile due to the low compressibility of water and have not been presented. Figure 3 b) compares the analytical and numerical solutions for two flow rates of vapour. A good match is achieved for both cases with maximum percentage errors of 0.07% and 0.4% for the 20 kg.m^{-2}s^{-1} and 400 kg.m^{-2}s^{-1} cases, respectively.

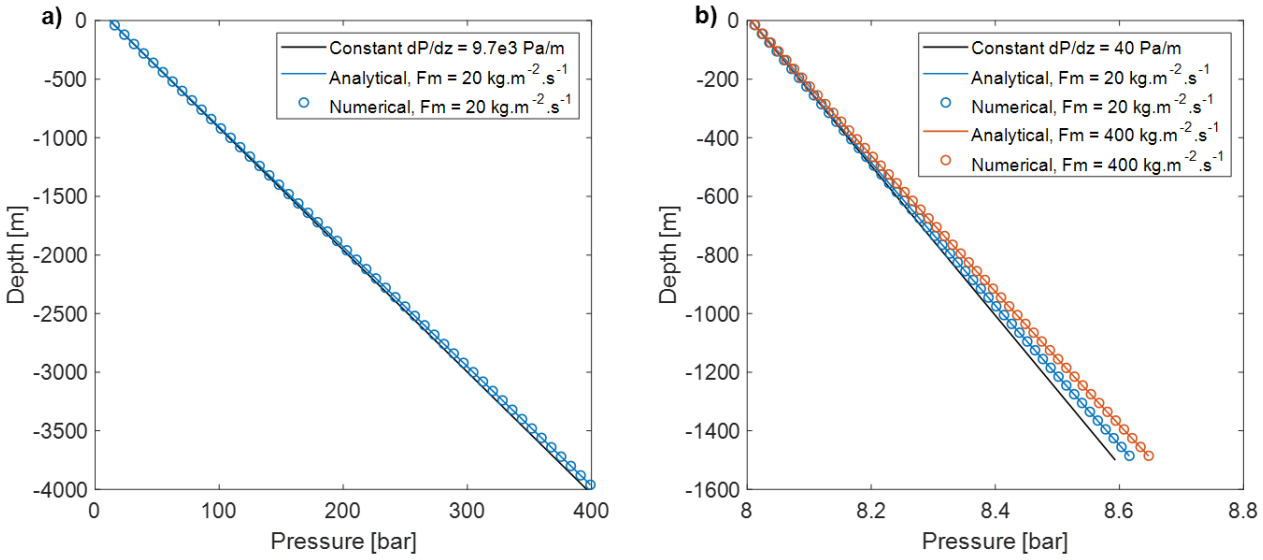

Figure 3: Numerical and analytical comparison for test case 2 for a) single-phase liquid and b) single-phase vapour

5.2 Test 3 - Ramey's Solution for Wellbore Heat Transport

Ramey (1962) presented an analytical approximation for wellbore temperatures during steam injection. Ramey's method was presented for geothermal applications by Horne and Shinohara (1979) for both production and injection cases. This method assumes the fluid has a constant density and heat capacity and that it is flowing at a steady rate. The reservoir was assumed to be radially symmetric and to have a constant vertical temperature gradient.

Both the liquid and vapour verification simulations were run with a reservoir thermal conductivity (k_{res}) of 2.422 W.m^{-1}.K^{-1} and an overall heat transfer coefficient *(U)* of 20 W.m^{-2}K^{-1}. Chiu and Thakur's (1991) time function, given in (10), was used to avoid the early time discontinuity that result from using Ramey's original time function. The liquid simulations were run with a wellhead pressure of 8 bar, a bottom-hole temperature of 175 °C and a bottom-hole mass flux of either 0 kg.m^{-2}.s^{-1}, 50 kg.m^{-2}.s^{-1} or 350 kg.m^{-2}.s^{-1}. For vapour simulations, a wellhead pressure of 8 bar and bottom-hole temperature of 300 °C were used. All simulations were run for 1.0e7 seconds.

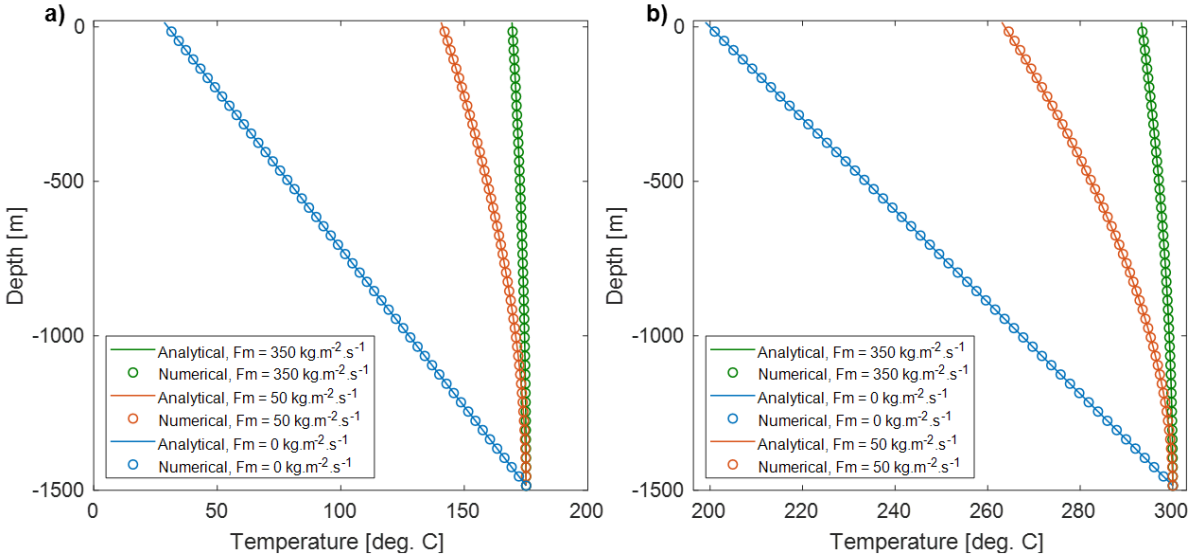

Figure 4: Numerical and analytical comparison for Ramey's solution for a) single-phase liquid and b) single-phase vapour

The reservoir temperature profiles varied linearly from 30 °C to 175 °C for liquid and from 200 °C to 300 °C for vapour. These profiles are shown by the 0 kg.m-2.s-1 cases in Figure 4. As expected, the wellbore temperature profile approaches the reservoir profile for a closed well. The flowing verification simulations matched the analytical solutions well. For liquid flow, the maximum difference between the analytical and simulated temperature values was 0.1% and 0.01% for the 50 $kg.m^{-2}.s^{-1}$ and 350 $kg.m^{-2}.s^{-1}$ cases, respectively. For vapour flow, the maximum difference was 0.08% and 0.01% for the 50 $kg.m^{-2}.s^{-1}$ and 350 $kg.m^{-2}.s^{-1}$ cases, respectively.

6. MODEL VALIDATION

Validation assesses the ability of the simulator to reproduce real-world observations. Two validation wells were chosen from the literature. Data for Well 6-1 from the East Mesa field, California was sourced from Ortiz-Ramirez (1983) and data for Well KJ-11 from the Krafla field, Iceland was sourced from Bjornsson (1987).

Well 6-1 is 2133 m deep with a uniform internal diameter of 0.2215 m. The well was discretized into 50 uniformly spaced elements. A bottom-hole pressure and temperature of 93 bar and 198.5 °C are used as boundary conditions in the bottom cell. The total mass flux is fixed at 335 $kgm^{-2}s^{-1}$ on the top boundary (wellhead). The shut-in wellbore temperature profile, given by Ortiz-Ramirez (1983), was used as a far-field reservoir temperature, and is shown in Figure 5 a). The wellbore completion and reservoir are assumed to have an overall heat transfer coefficient of 20 $W.m^{-2}K^{-1}$ and a thermal conductivity of 2.422 $W.m^{-1}.K^{-1}$, respectively. Figure 5 a) shows that the simulated steady-state profiles for Well 6-1 match the experimental data well with the average percentage between the recorded and simulated pressures and temperatures being 5.6% and 0.69%, respectively.

Well KJ-11 is a classic example of a well with multiple feed-zones, each with very different characteristics. Well testing indicated that feed-zones exist between 850-1050m, at 1500 m and below 1800m. Bjornsson (1987) presented multiple interpretations of the downhole data given in Figure 5 b). The case assuming influx from all sources was chosen as a validation case. KJ-11 was simulated to a depth of 2217m. An internal diameter of 0.214m for the top 750m and an internal diameter of 0.177m from 750m to the bottom-hole were used. A linear geothermal gradient from 30-295 °C was assumed, as shown in Figure 5 b). An overall heat transfer coefficient of 20 $W.m^{-2}K^{-1}$ and thermal conductivity of 2.422 $W.m^{-1}.K^{-1}$ were used. The wellhead pressure was fixed at 3 bar on the top boundary while mass influx was modelled using fixed source terms. The depth, mass flow, and enthalpy of each feed, estimated by Bjornsson (1987), are given in Table 2.

Figure 5b) presents the comparison between measured downhole data and the results of the simulation. The average difference between measured and simulated pressures was 27.8%. This is a result of an underestimated pressure gradient between 800 m and 1500 m. A good match has been achieved for the temperature profile with an average difference of 2.9% between the measured and the simulated values. These are deemed relatively good matches given the uncertainty in the conceptual model of the feed-zones in the well.

Table 2: Fixed reservoir source parameters for well KJ-11

Name	Depth [m]	Mass flow [kg/s]	Enthalpy [kJ/kg]
Feed 1	840 - 930	7.80	670
Feed 2	1730 - 1770	21.0	950
Feed 3	2180 - 2220	1.20	1312

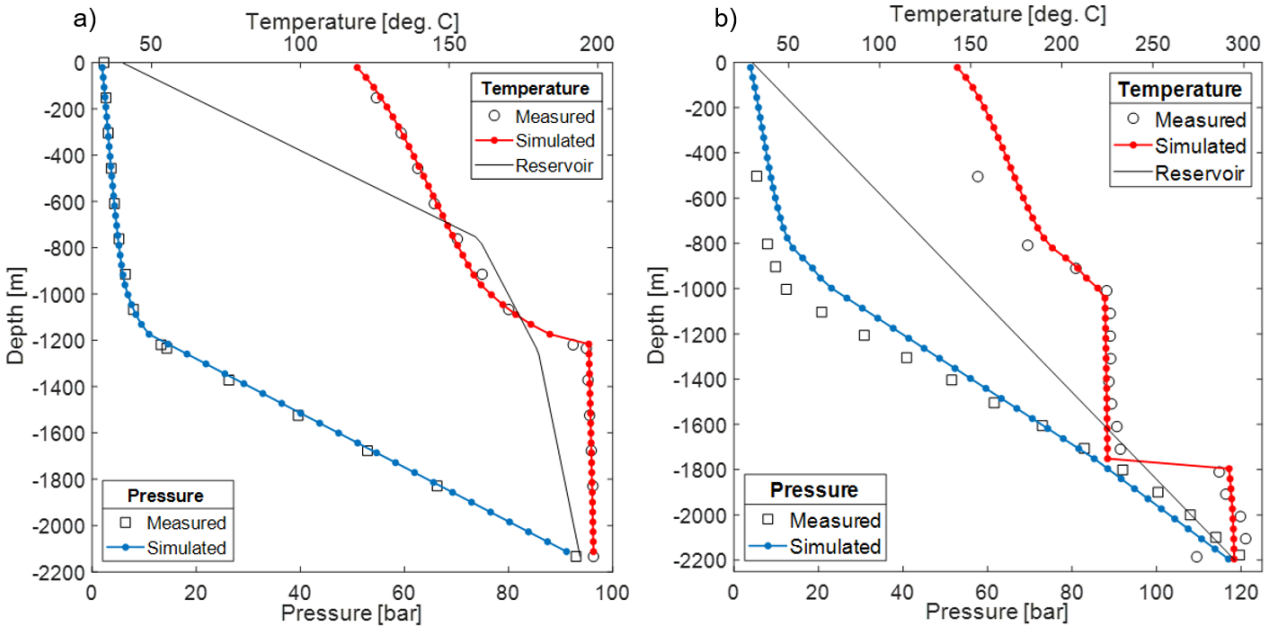

Figure 5: Comparison between measured and simulated PT profiles for a) East Mesa 6-1 and b) Krafla Kj-11

7. TRANSIENT MULTI-FEED EXAMPLE

The start-up process for a multi-feed well is presented here as an example of a challenging transient geothermal wellbore simulation. The wellbore structure, including the location of feed-zones and numerical discretization, was taken from the KJ-11 validation example given in Section 6. The wellbore radius and feed-zone locations are shown in Figure 6 c) and the feed-zone parameters are given in Table 3 below. Here, α is a lumped productivity index calculated for use in (14). The pressure, enthalpy, and productivity index assigned to each feed are artificial and do not represent the Krafla geothermal field. Instead, they were chosen to facilitate down-flow in the well.

The initial state of the wellbore is given in Figure 6 below. The well has a small positive mass flow of 0.2 kg/s leaking from the wellhead and internal circulation between the feed-zones. Fluid enters the well at Feed 1 flowing both up to the surface and down to Feeds 2 and 3. The initial wellbore temperature profile is significantly altered by this process and does not reflect the reservoir temperatures (a linear temperature profile between 30 and 295 °C).

Flow in the well is started by dropping the wellhead pressure from its initial values of 4.8 bar to a value of 2.5 bar. This value is held constant throughout the simulation. Zero velocity conditions are enforced on the bottom boundary and sources of mass and enthalpy vary based on the productivity indices provided in Table 3.

Figure 7 below shows profiles for pressure, temperature, saturation, and mass flow at various times during the simulation. Dropping the wellhead pressure stimulates flow within the wellbore. After 10 minutes, the increase in temperature at -1750m indicates production from Feed 2. Over the next 2.5 hours temperatures throughout the well slowly increase until, at 2:45 hours, the temperature has risen sufficiently for two-phase conditions to develop at the wellhead. Following this, the wellbore flashes rapidly due to the higher enthalpy fluid being produced from Feed 2. Over the next 15-minute period, the well flashes along a length of approximately 650 m. During this flashing process, large changes in the overall fluid density cause a significant drop in wellbore pressures and a large increase in the total mass flow rate. By 5:00 h, steady-state conditions are reached.

Although the above problem is relatively simple, it demonstrates the ability of the simulator to model situations with fast changes in fluid properties occurring over large sections of the well. Additionally, it highlights the use of a transient simulator to study the interaction between major feeds and how this affects the mass flow rate and enthalpy of the production fluid. This has significant implications for situations where production or re-injection processes induce internal circulation between major feeds.

Table 3: Source parameters for reservoirs on productivity

Name	Depth [m]	α [kg/s/Pa]	Pressure [bar]	Enthalpy [kJ/kg]
Feed 1	840 – 930	1.00E-06	95	770
Feed 2	1730 – 1770	3.20E-06	160	950
Feed 3	2180 – 2220	3.00E-07	185	1312

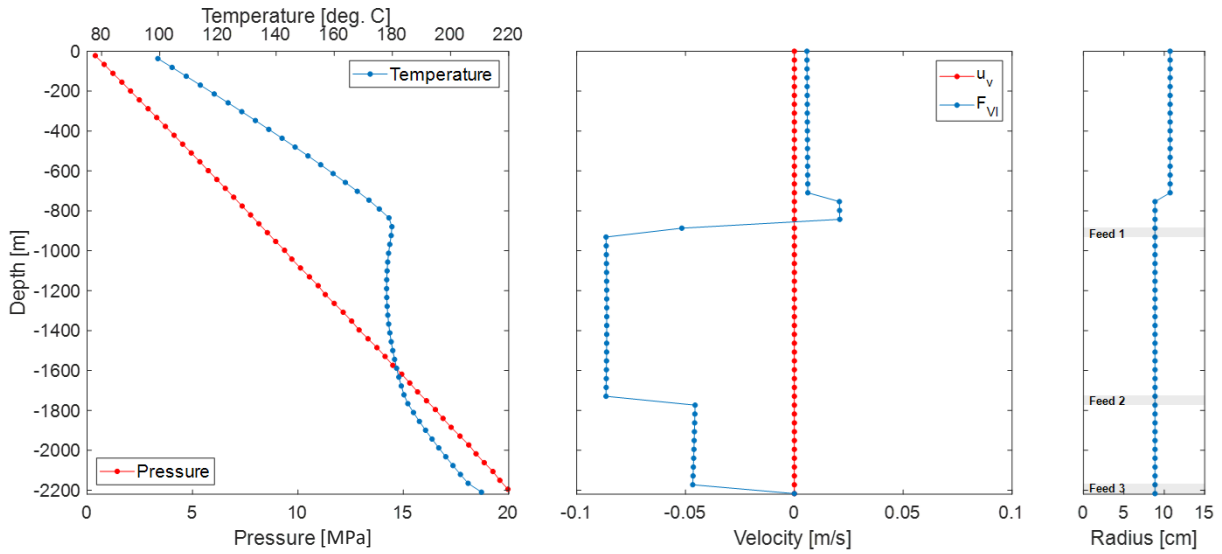

Figure 6: Initial state for a single-phase liquid wellbore with internal circulation, a) pressure and temperature, b) liquid and vapour velocities. c) Feed-zone location and wellbore radius.

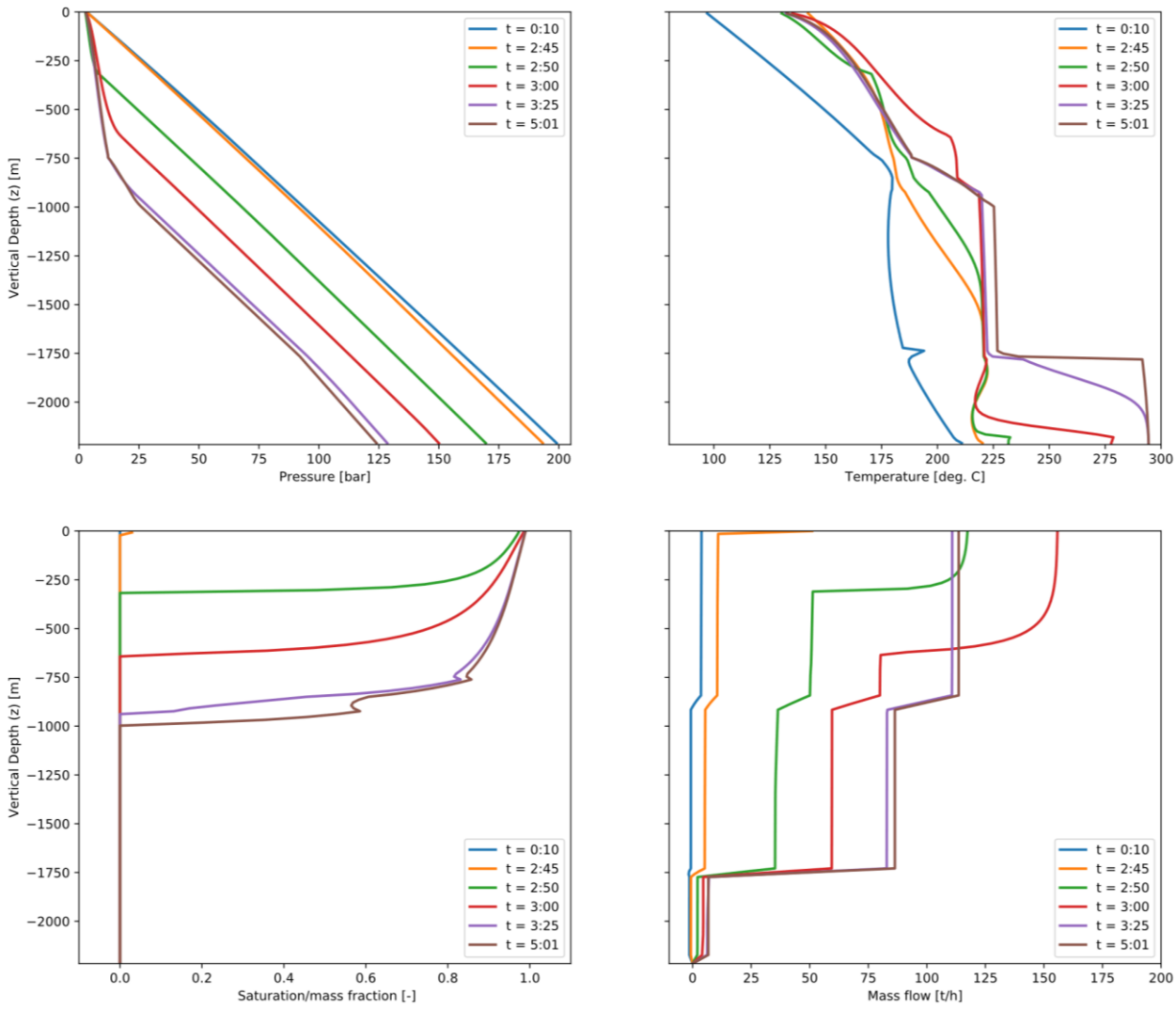

Figure 7: Simulated profiles for pressure, temperature, saturation, and mass flow during the start-up of the wellbore described in Section 7.

8. CHALLENGES FOR THE FUTURE

The understanding of key processes in geothermal engineering can be improved using transient wellbore simulations. Some examples are given below.

Transient well-test analysis infers reservoir characteristics from the measured pressure response due to changes in wellbore flow rate (Zarrouk and McLean, 2019). This transient pressure response is governed by a complex combination of reservoir and wellbore dynamics. Early investigations of well-testing using a wellbore simulator were completed by Miller (1980) and Miller et al. (1982), however, no further investigations have been completed. Although numerical reservoir simulations have been used to investigate these tests, the simulators used cannot account for complex well behavior (e.g., internal flow between feeds). Transient coupled simulations are required to understand these processes further.

Completion tests involve injecting cold water into wells at different flow rates. Permeable zones are then identified from PTS logs taken during testing. Internal circulation between feeds can affect the interpretation of these tests (Zarrouk and McLean, 2019). Transient, fully coupled simulations of the wellbore-reservoir system will improve understanding of these effects and improve the interpretation of test results. A transient wellbore simulator with multi-feed and counter-flow capabilities is required to model these tests.

Well deliverability may change in response to reservoir conditions. This process has been investigated infrequently using coupled wellbore-reservoir models. However, it is unclear whether the pseudo-transient, loose-lagged coupling used in these investigations can adequately model these processes. Transient, coupled simulations can be used to validate or improve current methods.

9. CONCLUSIONS

This paper outlines the initial development and testing of a transient, multi feed-zone, geothermal wellbore simulator. This included the presentation of the governing conservation equations, a clear statement of the assumptions made in their derivation, and an explanation of the additional constitutive equations required for model closure. The discrete formulation of the conservation equations, required for numerical solution, are discussed in detail. The simulator was verified against analytical solutions for very simple flows and validated against PT logs from both a single and multi-feed well. A test-case simulation that modelled the start-up processes of a multi-feed well, based loosely on KJ-11, was given. This demonstrated the ability of the simulator to model periods of intense flashing in the well and the resulting fast transients in saturation, pressure, and mass flow. Finally, some future applications of transient well models were briefly discussed

The development of this wellbore simulator is ongoing. Future work includes investigating the impact of different constitutive equations, particularly those governing slip and friction, on two-phase transient flow. Additionally, the simulator will be extended to include the effects of non-condensable gases. Finally, this simulator models the reservoir using simple productivity relationships. Improving the representation of the reservoir, using either radial flow equations or by coupling the wellbore to a numerical reservoir simulator, is required to deal with the future wellbore modelling challenges discussed above.

REFERENCES

Akbar, S., Fathianpour, N. and Al-Khoury, R.: A finite element model for high enthalpy two-phase flow in geothermal wellbores, *Renewable Energy*, **94**, (2016), 223–236.

Axelsson, G.: Geothermal Well testing, *Short Course V on Conceptual Modelling of Geothermal Systems* (2013).

Aunzo, Z. P., Bjornsson, G. and Bodvarsson, G. S.: *Wellbore Models GWELL, GWNACL, and HOLA User's Guide* (1991).

Beattie, D.: A Note on the Calculation of Two-Phase Pressure Losses, *Nuclear Engineering and Design,* **25**, (1973), 395–402.

Bendiksen, K. H., Maines, D., Moe, R., & Nuland, S.: The Dynamic Two-Fluid Model OLGA: Theory and Application. *SPE Production Engineering*, (1991).

Bjornsson, G.: *A Multi-Feedzone Geothermal Wellbore Simulator*. University of California, Berkeley (1987).

Chiu, K. and Thakur, S. C.: Modeling of Wellbore Heat Losses in Directional Wells under Changing Injection Conditions, *SPE Annual Technical Conference and Exhibition*, (1991), 517-528.

Chisholm, D.: Pressure gradients due to friction during the flow of evaporating two-phase mixtures in smooth tubes and channels, *International Journal of Heat and Mass Transfer*, **16**, (1973), 347–358.

García-Valladares, O., Sánchez-Upton, P. and Santoyo, E.: Numerical modeling of flow processes inside geothermal wells: An approach for predicting production characteristics with uncertainties, *Energy Conversion and Management*, (2006), 1621-1643.

Gudmundsdottir, H. and Jonsson, M. T.: The Wellbore Simulator FloWell – Model Enhancement and Verification, P*roceedings,* World Geothermal Congress 2015, Melbourne, AUS (2015).

Freeston, D. H. and Gunn, C. 'Wellbore Simulation - Case Studies', in *Eighteenth Workshop on Geothermal Reservoir Engineering Stanford University*. Stanford, (1993), pp. 261–266.

Horne, R. N. and Shinohara, K.: Wellbore Heat Loss in Production and Injection Wells, *J Pet Technol*, **31**, (1979), 116-118.

Itoi, R., Katayama, Y., Tanaka, T., Kumagai, N. and Iwasaki, T.: Numerical Simulation of Instability of Geothermal Production Well, *Geothermal Resource Counsel Transactions*, **37**, (2013), 837–842.

Khasani, Jalilinasrabady, S., Fujii, H. and Itoi, R.: Numerical study on the effects of wellhead restriction modes on the transient behaviors of a geothermal well deliverability applicable for short period of measurement, *Geothermics*, **69**, (2017), 34–44.

Marquez, S., Sazon, T. and Omagbon, J.: SIMGWEL : EDC's New Geothermal Wellbore Modeling Software, *Proceedings*, World Geothermal Congress 2015, Melbourne, AUS (2015).

Mcguinness, M. J.: SwelFlo User Manual, Wellington, NZ (2015).

Miller, C.: *Wellbore User's Manual*, University of California, Berkeley, CA (1980).

Miller, C.: Wellbore Storage Effects in Geothermal Wells, *Society of Petroleum Engineers Journal*, (1980), 555–566.

Miller, C., Benson, S., O'Sullivan, M. and Pruess, K.: Wellbore Effects in the Analysis of Two-Phase Geothermal Well Tests, *Society of Petroleum Engineers Journal,* **22** , (1982), 309–320.

Ortiz-Ramirez, J.: Two-Phase Flow in Geothermal Wells: Development and Uses of a Computer Code (1983).

Pan, L., Freifeld, B., Doughty, C., Zakem, S., Sheu, M., Cutright, B. and Terrall, T.: Fully coupled wellbore-reservoir modeling of geothermal heat extraction using CO2 as the working fluid, *Geothermics*, **53**, (2015), 100-113.

Pan, L. and Oldenburg, C. M.: T2Well - An integrated wellbore-reservoir simulator, *Computers and Geosciences*, **65**, (2014), 46–55.

Pan, L., Webb, S. W. and Oldenburg, C. M.: Analytical solution for two-phase flow in a wellbore using the drift-flux model, *Advances in Water Resources*, **34**, (2011), 1656–1665.

Ramey, H. J.: Wellbore Heat Transmission, *Journal of Petroleum Technology*, **14**, (1962), 427–435.

Revised Release on the Surface Tension of Ordinary Water Substance, In *International Association for the Properties of Water and Steam*, (2014).

Shi, H. Holmes, J., Durlofsky, L., Aziz, K., Diaz, L., Alkaya, B and Oddie, G.: Drift-Flux Modeling of Two-Phase Flow in Wellbores, *SPE Journal*. Society of Petroleum Engineers, **10**, (2005), 24–33.

Tonkin, R. O'Sullivan, J. and O'Sullivan, M. On the Choice of Primary Variables in Geothermal Wellbore modelling. Proc. 42nd New Zealand Geothermal Workshop, Waitangi, NZ (2020).

Upadhyay, R., Hartz, J., Tomkoria, B. and Gulati, A.: Comparison Of Calculated And Observed Pressure Drops In Geothermal Wells Producing Steam-Water Mixtures. 52nd Annu. Fall Tech. Conf. Exhib. Soc. Pet. Eng., (1977), 1–10.

Vasini, E., Battistelli, A., Berry, P., Bonduà, S., Bortolotti, V., Cormio, C. and Pan, L.: Interpretation of production tests in geothermal wells with T2Well-EWASG., *Geothermics*, **73**, (2018), 158–167.

Vijayan, P. K., Patil, A. P., Pilkhwal, D. S., Saha, D. and Venkat Raj, V.: Assessment of pressure drop and void fraction correlations with data from two-phase natural circulation loops, *Heat and Mass Transfer*, **36**, (2000), 541–548.

Wagner, W., Cooper, J. R., Dittmann, A., Kijima, J., Kretzschmar, H. J., Kruse, A., Mares, R., Oguchi, K., Sato, H., Stocker, I., Sifner, O., Takaishi, Tanishita, I., Trubenbach, J., & Willkommen, T. IAPWS Industrial Formulation 1997 for the Thermodynamic Properties of Water and Steam. *Transactions of the ASME*, (2000), 150–182.

Willhite, G. P.: Over-all Heat Transfer Coefficients in Steam and Hot Water Injection Wells, *Journal of Petroleum Technology*, (1967).

Yamamura, K., Itoi, R., Tanaka, T. and Iwasaki, T.: Numerical Analysis of Transient Steam-Water Two-Phase Flow in Geothermal Production Wells with Multiple Feed Zones, *Proceedings*, 42nd Workshop on Geothermal Reservoir Engineering Stanford University, Stanford, CA (2017).

Yadigaroglu, G., & Hewitt, G. F. Introduction to Multiphase Flow (G. Yadigaroglu & G. F. Hewitt (eds.)), (2018).

Zarrouk, S. J. and McLean, K.: *Geothermal Well Test Analysis: Fundamentals, Applications and Advanced Techniques*. (2019).

Zuber, N. and Findlay, J. A.: Average Volumetric Concentration in Two-Phase Flow Systems, *Journal of Heat Transfer*. ASME, **87**, (1965), 453–468.